Supporting Information

Materials and Methods

Materials

Polyethylene (PE) was supplied by Alfa Aesar (China) Chemical Co. Ltd. Tetrapropylammonium hydroxide (TPAOH, 25 *wt*%) was supplied by Shanghai Cairui Chemical Co. Ltd. Aluminum isopropoxide [$Al(C_3H_7O)_3$] was purchased from Rhawn Co. Urea, pyridine, and zinc nitrate ($Zn(NO_3)_2 \cdot 6H_2O$) were obtained from Sino-Pharm Chemical Reagent Co. Ltd. Tetraethyl orthosilicate (TEOS), sodium hydroxide (NaOH), and CH_2Cl_2 were purchased from Aladdin Industrial Co. N_2, CH_4, C_3H_6, and H_2/Ar were supplied by Hangzhou Jingong Special Gas Co. Ltd. ZSM-5 zeolites was provided by Tianjin Nanhua Catalyst Ltd. These raw materials for preparing catalysts were analytical grade and used directly without further treatment.

Characterizations

X-ray diffraction (XRD) spectra of the zeolites were collected on a Rigaku Ultimate IV diffractometer with Cu curved monochromator and using Cu-Kα-radiation (λ=1.5418 Å). Nitrogen sorption isotherms were measured at -196 °C using a Micromeritics ASAP 2020M and 3020M system to calculate the micropore volume, external and specific surface area. The Brunauer-Emmett-Teller (BET) surface areas were calculated from the adsorption data. Surface areas were calculated using the BET equation. Micropore volume and external surface area were calculated using the t-plot method with the Jura-Harkins equation for determining the thickness of the adsorbed layer. The samples were previously outgassed at 300 °C for 3 h under vacuum before the measurements. The size and morphology of the zeolite crystals were determined by scanning electron microscopy (SEM) using a Hitachi SU-8010 electron microscopy. Transmission electron microscopy (TEM) and energy dispersive spectroscopy (EDS) elemental maps were performed on a Hitachi H-9500 electron microscope with an acceleration voltage of 200 kV. Si/Al ratios were measured with inductively coupled plasma (ICP) analysis over Perkin-Elmer 3300DV. Thermogravimetric analysis (TG) was obtained with a SDT Q600 V8.2 Build 100 instrument in air at a heating rate of 10 °C/min. Temperature-programmed desorption of ammonia (NH_3-TPD) curve was carried out on a Micromeritics ChemiSorb 2720 Pulse Chemisorption System. The weighed sample (100 mg) was pretreated at 450 °C for 3 h under O_2 and 1 h under He, then cooled to 20 °C. The NH_3-He (10 vol% NH_3) gas was introduced at 100 °C for 1 h to ensure the saturation adsorption of NH_3. The sample was then purged with He for 1 h until the signal returned to the baseline as monitored by a thermal conductivity detector (TCD). For the temperature-programmed oxidation (TPO) measurement, 20 mg of sample was sandwiched between quartz wool to prevent scattering and are subsequently packed into a quartz reaction tube. The quartz reaction tube was placed in an electric furnace. The samples were heated to 700 °C at a heating rate of 20 °C /min under a mixture atmosphere of 10%O_2/He (flow rate: 10mL/ min). The carbon species of the sample were then released as CO_2 and measured on a mass spectrum (SRD200M, TILONGRP TECHNOLOGY LIMITED) instrument. Raman spectra were recorded using an HR800 Raman spectrometer equipped with an Ar excitation source (λ = 514.532 nm). ^1H and ^{13}C NMR of the liquid product spectra were recorded on Bruker Avance-500 (500 MHz) spectrometer and were analyzed using MestReNova. Chemical shifts (δ, ppm) were calibrated using the residual proton signals of the solvent and referenced to tetramethyl silane (TMS, δ=0 ppm).

Product analysis

Gas chromatography. The liquid and gaseous products were obtained by the cold bath and gas collector, respectively, and then analyzed by GC and further confirmed by GC-MS (diluted with CH_2Cl_2). After the reaction, the reaction tube and cold bath were washed with CH_2Cl_2 to collect all the liquid products, and an internal standard was added to

analyze the liquid products using a gas chromatography (Fuli-1690) equipped with a flame ionization detector (FID) and HP-5 column. The gaseous products in the gas collector were analyzed by gas chromatography (Fuli-1690) equipped with a flame ionization detector (FID) and PLOT-Al_2O_3 column, using methane as an internal standard. The gaseous products were analyzed both before and after injecting the methane internal standard to avoid the influence of methane products from the polymer depolymerization. The products were further confirmed by GC-MS analysis (SHIMADZU-GCMS-QP2010SE).

We used two internal standards of mesitylene and bromobenzene for quantifying the product yields, which provided the same data within error bounds, confirming the accuracy of product analysis following these methods. The details for quantifying liquid products are in the following.

(i) method using mesitylene internal standard

After the reaction, the liquid products were collected in a cold bath, the content of each component in the was analyzed by GC with mesitylene as an internal standard. The mixture was analyzed using GC before and after adding the mesitylene, and their yields were calculated as follows:

$$\text{Yield} = \frac{\sum \Delta m * f * S_i / \Delta S}{m_{PE}}$$

Where Δm is the mass of the internal mesitylene, f is relative correction factor (mass basis), S_i is the area of hydrocarbon molecule with carbon number at i, while ΔS is the area difference of mesitylene before and after adding to the internal, and m_{PE} is mass of the initial reactant PE.

ΔS was calculated following a peak-area-normalization method to avoid influence by fifference in each sample injection to GC, following the equation

$$\Delta S = S'_{mesitylene} - \frac{S'_{toluene}}{S_{toluene}} \times S_{mesitylene}$$

$S_{mesitylene}$ and $S'_{mesitylene}$ is the area of mesitylene before and after adding the internal. $S_{toluene}$ and $S'_{toluene}$ is the area of toluene before and after adding the internal.

(ii) method using bromobenzene internal standard

To verify the accuracy of the above calculation, another internal bromobenzene was added, where the of each product could be directly obtained following the general internal standard method. The yield of each compounds products in the liquid was calculated as

$$\text{Yield} = \frac{\sum \Delta m' * f' * S_i / S_{Br}}{m_{PE}}$$

Where $\Delta m'$ is mass of the internal bromobenzene, f' is relative correction factor (mass basis), S_i is the area of hydrocarbon molecule with carbon number at i, while S_{Br} is the area of bromobenzene, and m_{PE} is mass of the initial reactant PE.

NMR spectroscopy. Spectra of the products were recorded in $CHCl_3$-d2. ^1H and ^{13}C NMR of the liquid product spectra were recorded on Bruker Avance-500 (500 MHz) spectrometer and were analyzed using MestReNova. Chemical shifts (δ, ppm) were calibrated using the residual proton signals of the solvent and referenced to tetramethyl silane (TMS, δ=0 ppm).

Catalytic conversion of C_3H_6. The reaction was carried out in a fixed-bed reactor. All the catalyst was sieved through a 40–60 mesh. 400 mg of quartz sand and 400 g of catalyst were physically mixed and localized within the middle of the reaction tube, which was heated to (400 ± 5) °C under N_2 (at a constant atmospheric pressure) in a quartz tube. Then, 10% C_3H_6/90% N_2 was induced to the reactor with a flow rate at 10 mL/min, which lasted for 4 h. The temperature of the catalyst bed was maintained at (400 ± 5) °C. The products were separated by a condensing collector. The liquid and gaseous products were obtained by the cold bath and gas collector, respectively, and then analyzed by

GC and further confirmed by GC-MS (diluted with CH_2Cl_2). C_3H_6 conversion was calculated by the internal standard method with methane.

Thermodynamic analysis of aromatization

The thermodynamic feasibility of the reaction was assessed using data computed from the Benson group increment theory. Increment values are compiled in Table S2. According to the additivity of group properties,[1-3] the alkane group values ($g_{A,n}$) decreased with the increase of molecular number (n), in which case the group values of linear polyethylene is very low (S1). According to the results of GPC, the number-average molecular weight of the PE is about 28481 g mol^{-1}, so n is about 2000.

The thermodynamic contributions to a linear alkane C_nH_{2n+2} are as follows:

$$g_{A,n}=(n-2)g_1+2g_2 \quad \text{(S1)}$$

Compared with alkanes, there is a comparatively large number of values of the heats of formation of alkenes. The thermodynamic contributions to a linear light olefin C_mH_{2m} are as follows:

$$g^{=}_{A,m}=(m-4)g_1 + g_2+ g_3+ g_4+ g_5 \quad \text{(S2)}$$

The enthalpy of methylated aromatics is much higher than that of the alkanes and alkenes. Take xylene for example, the thermodynamic contributions are as follows:

$$g_x =2g_2+2g_6+4g_7+g_8 \quad \text{(S3)}$$

For the direct conversion of polyethylene to xylene (eq 1), the thermodynamic contributions are as follows:

$$C_{8n}H_{16n+2} \rightarrow nC_8H_{10} +(3n +1) H_2 \ (8n\approx2000) \quad \text{(eq1)}$$

$$g_{Ar,x} = (3n +1)g_H + 2n\, g_2 + 2ng_6 + 4ng_7 + ng_8- (8n-2)g_1-2g_2 = n(3g_H + 2g_2 + 2g_6 + 4g_7 +g_8 - 8g_1) + g_H -2g_2 +2g_1 \quad \text{(S4)}$$

For the conversion of light olefin to xylene, for example, butene (eq 2), the thermodynamic contributions are:

$$2C_4H_8 \rightarrow C_8H_{10} +3H_2 \quad \text{(eq2)}$$

$$g_{Ar,y} = 3g_H + 2\, g_2 + 2g_6 + 4g_7+g_8 – 2(\, g_2+ g_3+ g_4+ g_5) = 3g_H - 2g_3- 2g_4- 2g_5+ 2g_6 + 4g_7 +g_8 \quad \text{(S5)}$$

For propylene (eq 2), the thermodynamic contributions are as follows:

$$8C_3H_6 \rightarrow 3C_8H_{10} +9H_2 \quad \text{(eq3)}$$

$$g_{Ar,y} = 9g_H + 6g_2 + 6g_6 + 12g_7+3g_8 – 8(\, g_2+ g_3+ g_4) = 9g_H - 2g_2- 8g_3- 8g_4+ 6g_6 + 12g_7 +3g_8 \quad \text{(S5)}$$

Without H_2, the thermodynamic contributions for the alkane cracking reaction are as follows:

$$C_{m+n}H_{2m+2n+2} \rightarrow C_mH_{2m} + C_nH_{2n+2} \quad \text{(eq4)}$$

$$g_{m,n} = g^{=}_{A,m} + g_{A,n} - g_{A,m+n} = -4g_1 + g_2+ g_3+ g_4+ g_5 \quad \text{(S9)}$$

For the hydrogenation of light olefin to alkanes, for example, butene (eq 5), the thermodynamic contributions are as follows:

$$C_4H_8 + H_2 \rightarrow C_4H_{10} \quad \text{(eq5)}$$

$$g_H = g_1 + g_2- g_3- g_4 \quad \text{(S10)}$$

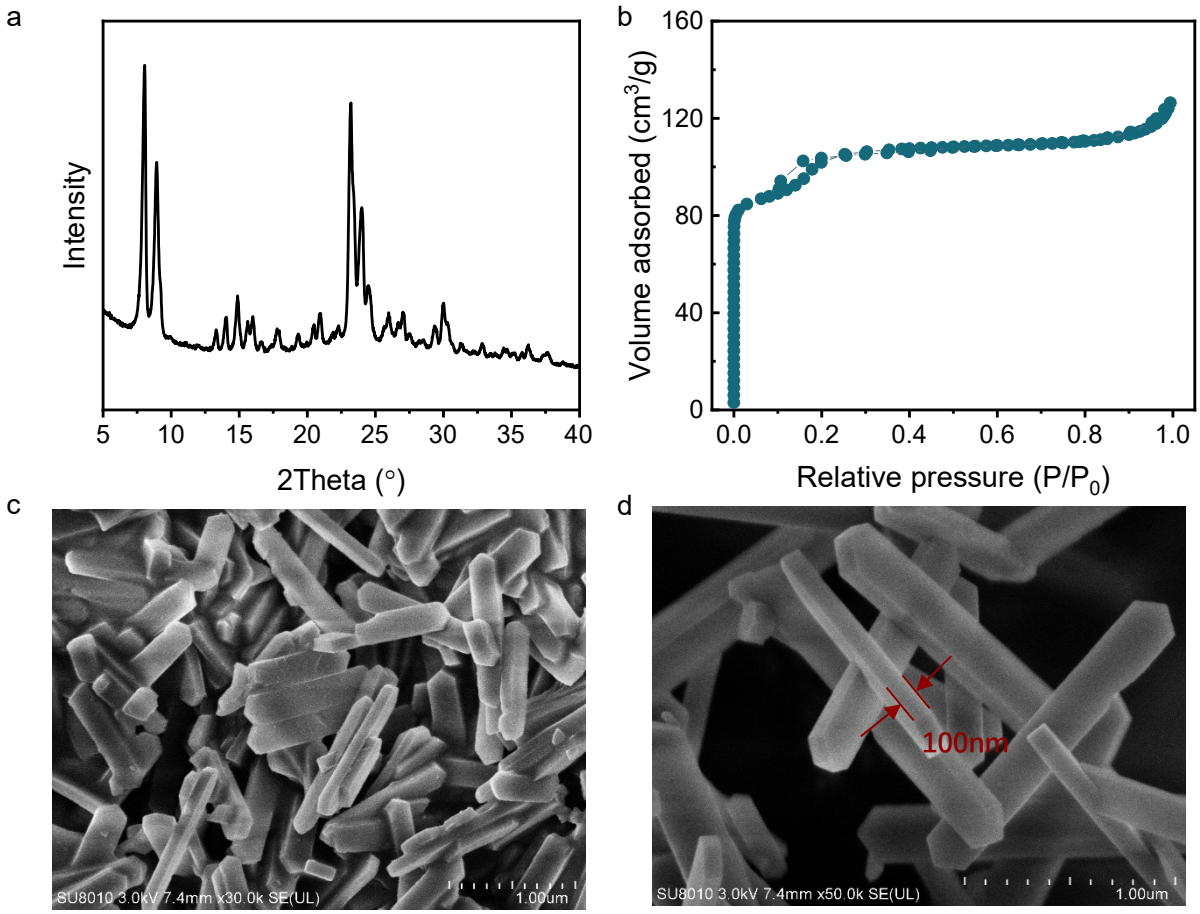

Figure S1. (a) XRD pattern, (b) N_2 sorption isotherms, and (c,d) SEM images of *s*-ZSM-5. The surface area was 390.7 m^2/g.

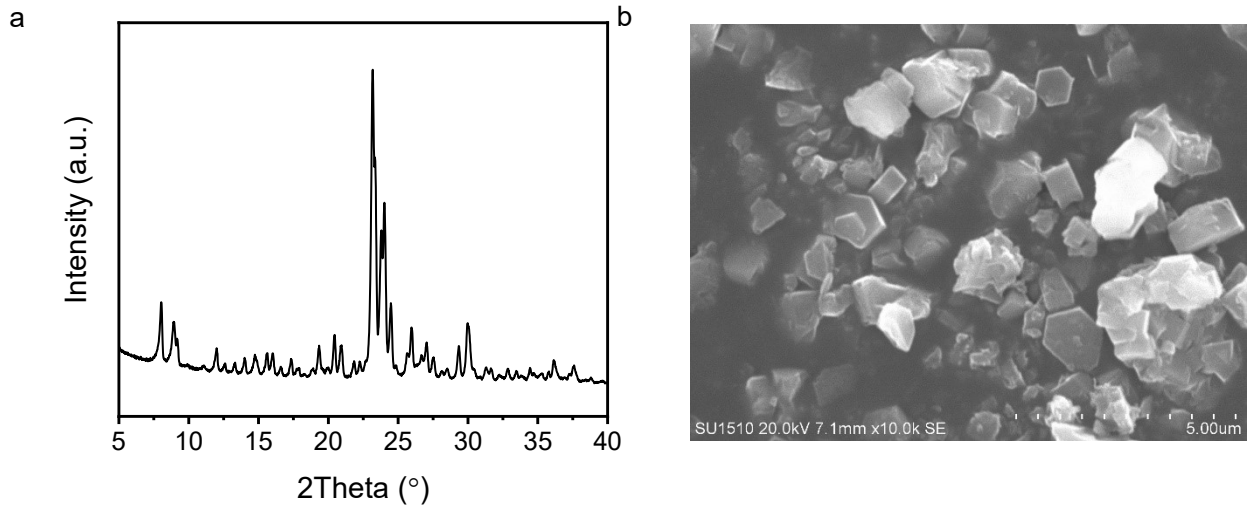

Figure S2. (a) XRD pattern and (b) SEM image of Zn/ZSM-5.

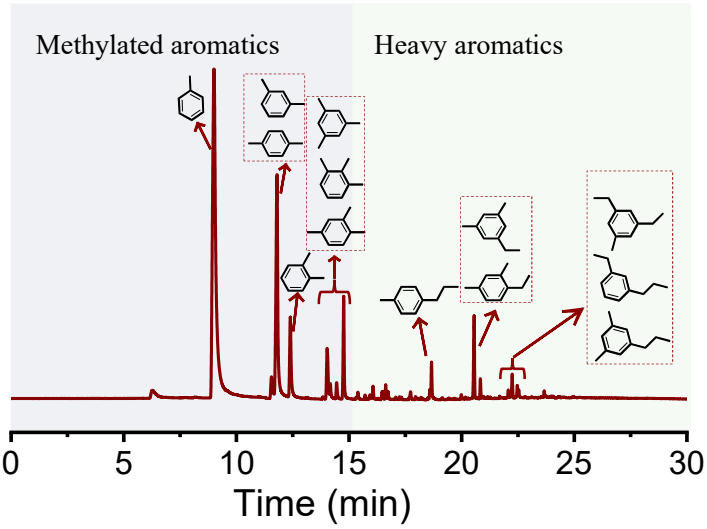

Figure S3. GC curves analyzing the liquid products for *s*-ZSM-5 and Zn/ZSM-5 catalyst. Reaction conditions: 500 mg of PE, 100 mg of *s*-ZSM-5, and 400 mg of Zn/ZSM-5, feed gas of 3.3% H_2/29.7% Ar/67% N_2, a flow rate of 3 mL/min, 400 °C, reaction for 4 h.

Figure S4. Photographs of the spent (a) *s*-ZSM-5+Zn/ZSM-5, (b) *s*-ZSM-5+Zn/*meso*-ZSM-5. Reaction conditions: the mixture of 500 mg of PE and 100 mg of *s*-ZSM-5 in the first bed, 400 mg of catalyst for aromatization in the second bed, feed gas of 3.3% H_2/29.7% Ar/67% N_2, a flow rate of 3 mL/min, 400 °C, 4 h.

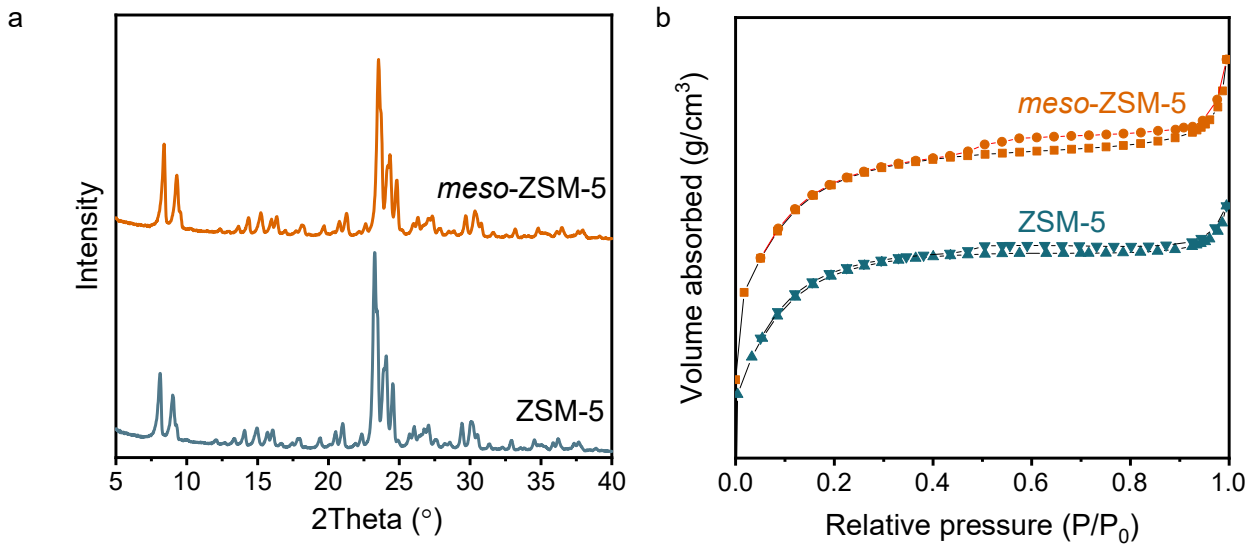

Figure S5. (a) XRD patterns and (b) N_2 sorption isotherms of ZSM-5 and *meso*-ZSM-5 zeolite. The surface areas of ZSM-5 and *meso*-ZSM-5 zeolite were 327.7 m^2/g and 370.9 m^2/g

Note: As shown in Figure S6a, in both tests by mixing the PE feed with *meso*-ZSM-5 (mono-bed) and packing *meso*-ZSM-5 under the mixture of PE and s-ZSM-5 (dual-bed), low yields of aromatics were obtained. This phenomenon is due to the rapid coke formation in the *meso*-ZSM-5 zeolite (Figure S6b and S6c**)**, which failed to efficiently catalyze the aromatization step.

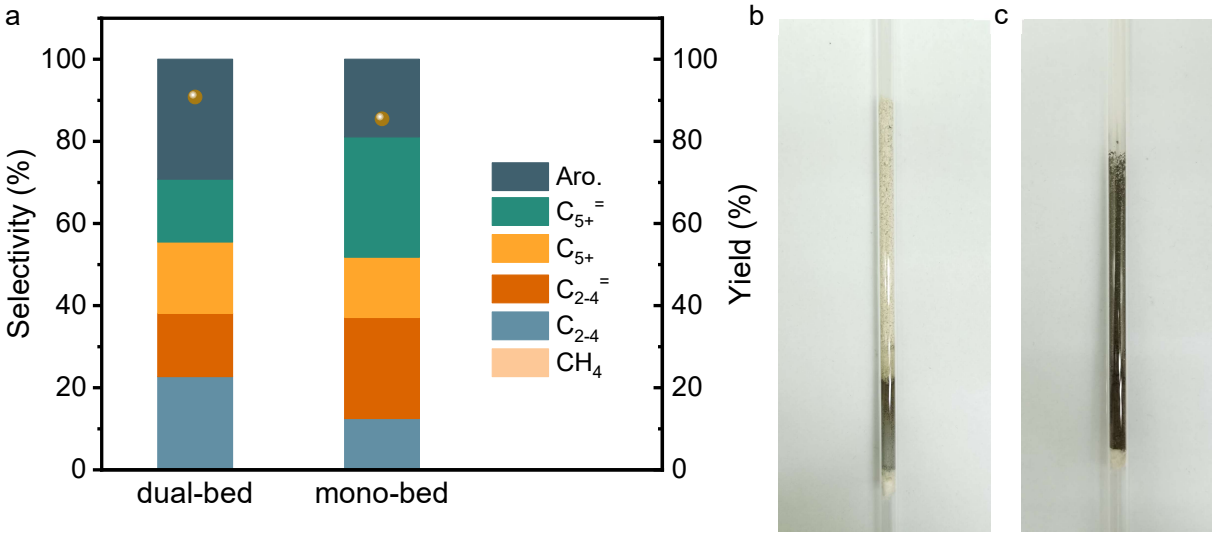

Figure S6. (a) Data characterization of polyethylene aromatization over *s*-ZSM-5 and *meso*-ZSM-5 catalysts. The dual-bed reaction conditions: a mixture of 500 mg of PE and 100 mg of *s*-ZSM-5 in the first bed, 400 mg of *meso*-ZSM-5 for aromatization in the second bed, feed gas of 3.3% H_2/29.7% Ar/67% N_2, a flow rate of 3 mL/min, 400 ° C, 4h. The mono-bed reaction conditions: a mixture of 500 mg of PE and 100 mg of *meso*-ZSM-5, feed gas of 3.3% H_2/29.7% Ar/67% N_2, a flow rate of 3 mL/min, 400 °C, 4h. Photographs of the spent (b) *s*-ZSM-5+ *meso*-ZSM-5 and (b) *meso*-ZSM-5 catalysts after the tests.

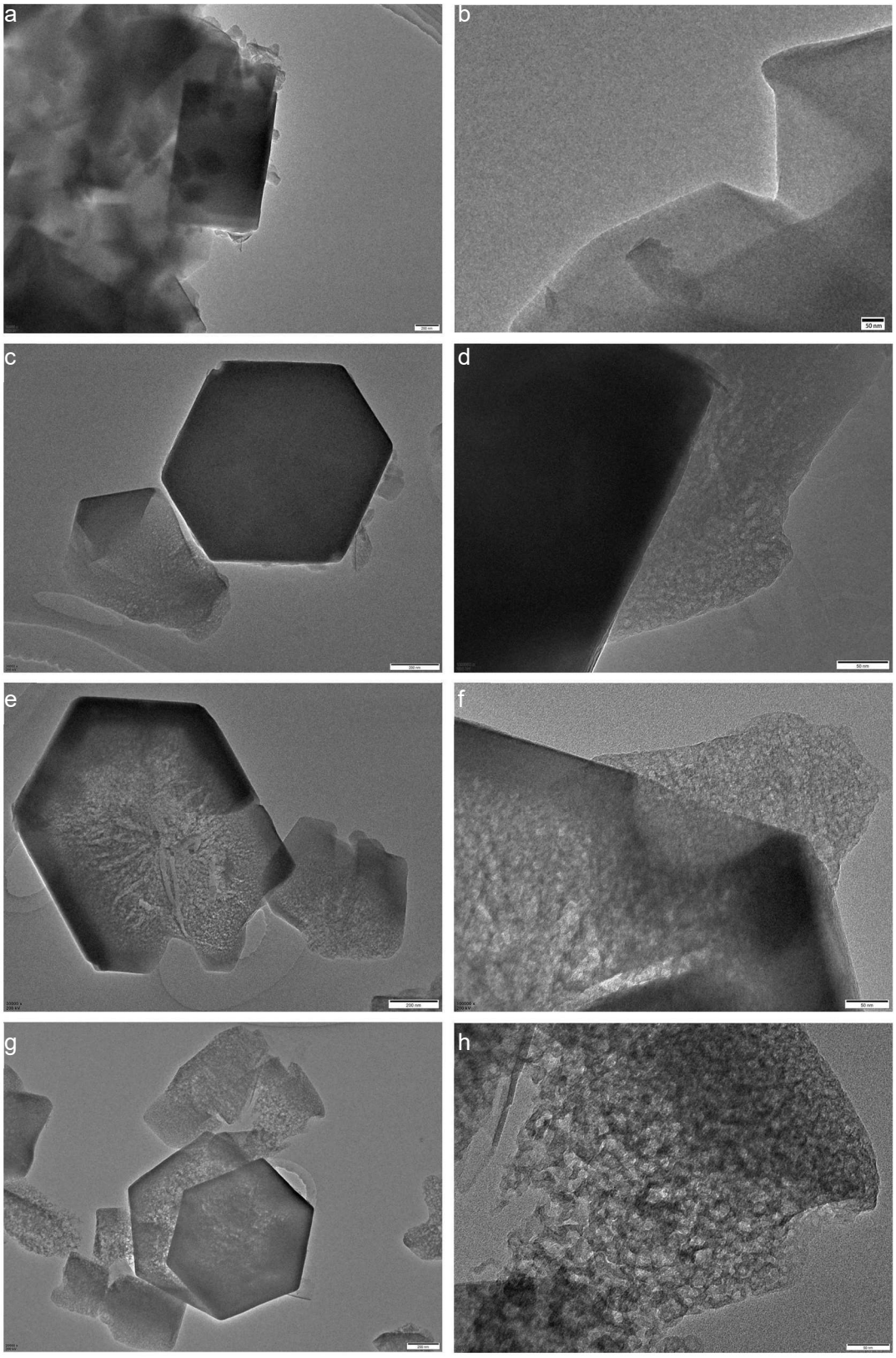

Figure S7. TEM images of (a, b) commercial ZSM-5, and this zeolite treated by (c, d) 0.2 M NaOH, (e, f) 0.5 M NaOH, and (g, h) 0.8 M NaOH aqueous solution.

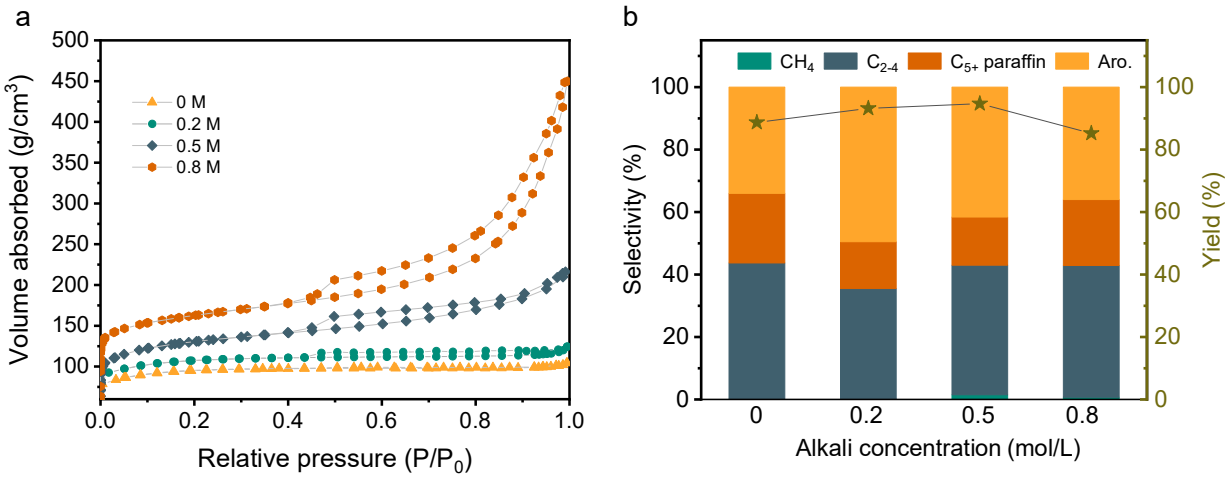

Figure S8. (a) N_2 sorption isotherms of ZSM-5 and *meso*-ZSM-5 zeolite treated with different NaOH concentrations. (b) Data characterization of the aromatization of PE over Zn/*meso*-ZSM-5 zeolite treated with different NaOH concentrations. Reaction conditions: the mixture of 500 mg of PE and 100 mg of *s*-ZSM-5 in the first bed, 400 mg of Zn/*meso*-ZSM-5 treated with different NaOH concentrations in the second bed, feed gas of 3.3% H_2/29.7% Ar/67%N_2, a flow rate of 3 mL/min, 400 °C, 4h.

Note: Even with the nitrogen sorption parameters of the *meso*-ZSM-5 was not changed so obviously, it still exhibited enhanced performances compared with the commercial ZSM-5 in the cascade catalysis. Similar phenomena are in good agreement with that in the previous study.[4-8] For example, Ma and co-workers obtained the *meso*-ZSM-5 by a treatment using 0.1 M aqueous NaOH solution, resulting in the sample with similar nitrogen sorption parameters but different performances in the syngas-to-aromatics conversion.[5] Svelle reported that the textural properties of ZSM-5 were not obviously changed after treatment by 0.05 M aqueous NaOH solution, but an obviously increased selectivity for C_{6+} products and a longer lifetime was achieved in the conversion of methanol.[7]

In addition, we further performed the alkaline treatment of ZSM-5 zeolite using 0.5 and 0.8 M aqueous NaOH solution, which is sufficient to get the *meso*-ZSM-5 with more mesopores that result in more obviously changed nitrogen sorption parameters (Figure S8a and Table S1). For example, the mesopore volumes were increased to 0.17 and 0.36 cm^3/g by treatment using 0.5 and 0.8 M aqueous NaOH solution, respectively. We studied their performances in the PE conversion by combining them with *s*-ZSM-5 zeolite in cascade catalysis. The yield of aromatics in the test using *meso*-ZSM-5 treated with 0.5 and 0.8 M aqueous NaOH solution was still lower than that with 0.2 M aqueous NaOH solution, because the aromatization was influenced by both porosity and acidity (Figures S7b and S9). For example, the treatment with 0.8 M aqueous NaOH solution formed the most mesopores among these samples, but the acids were seriously lost because of the damage to the zeolite framework by desilication. As a result of catalysis, the *meso*-ZSM-5 obtained using 0.8 M NaOH gave a lower yield to aromatic products. This trend is also in good agreement with the previous results in aromatization.[9-13]

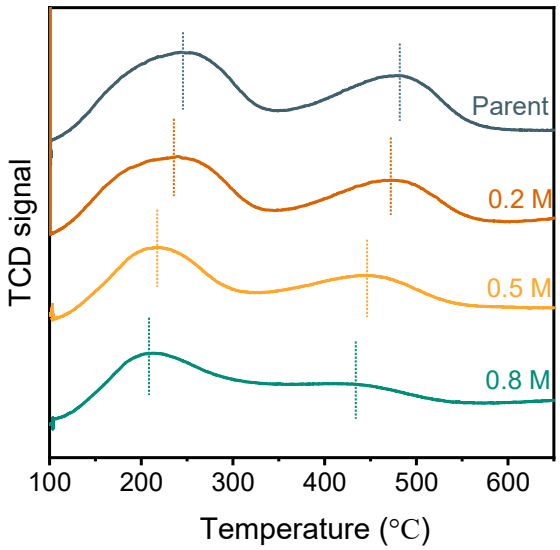

Figure S9. NH_3-TPD profiles of *meso*-ZSM-5 treated with different concentrations of aqueous NaOH solution.

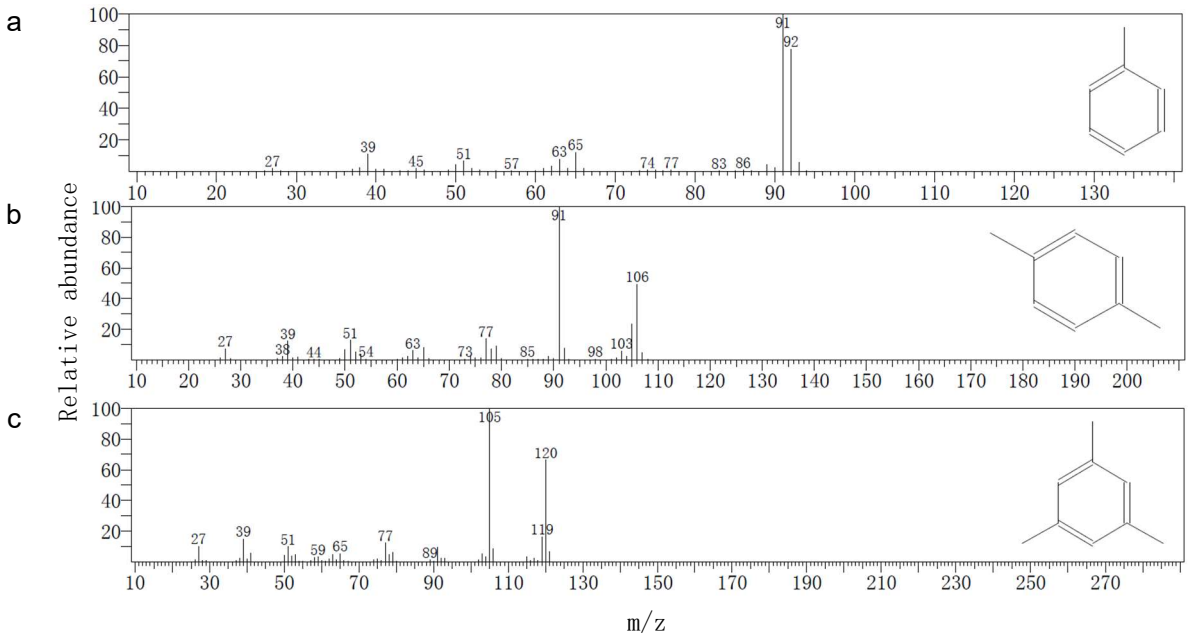

Figure S10. GC-MS analysis of the main products of (a) toluene, (b) xylene, and (c) mesitylene.

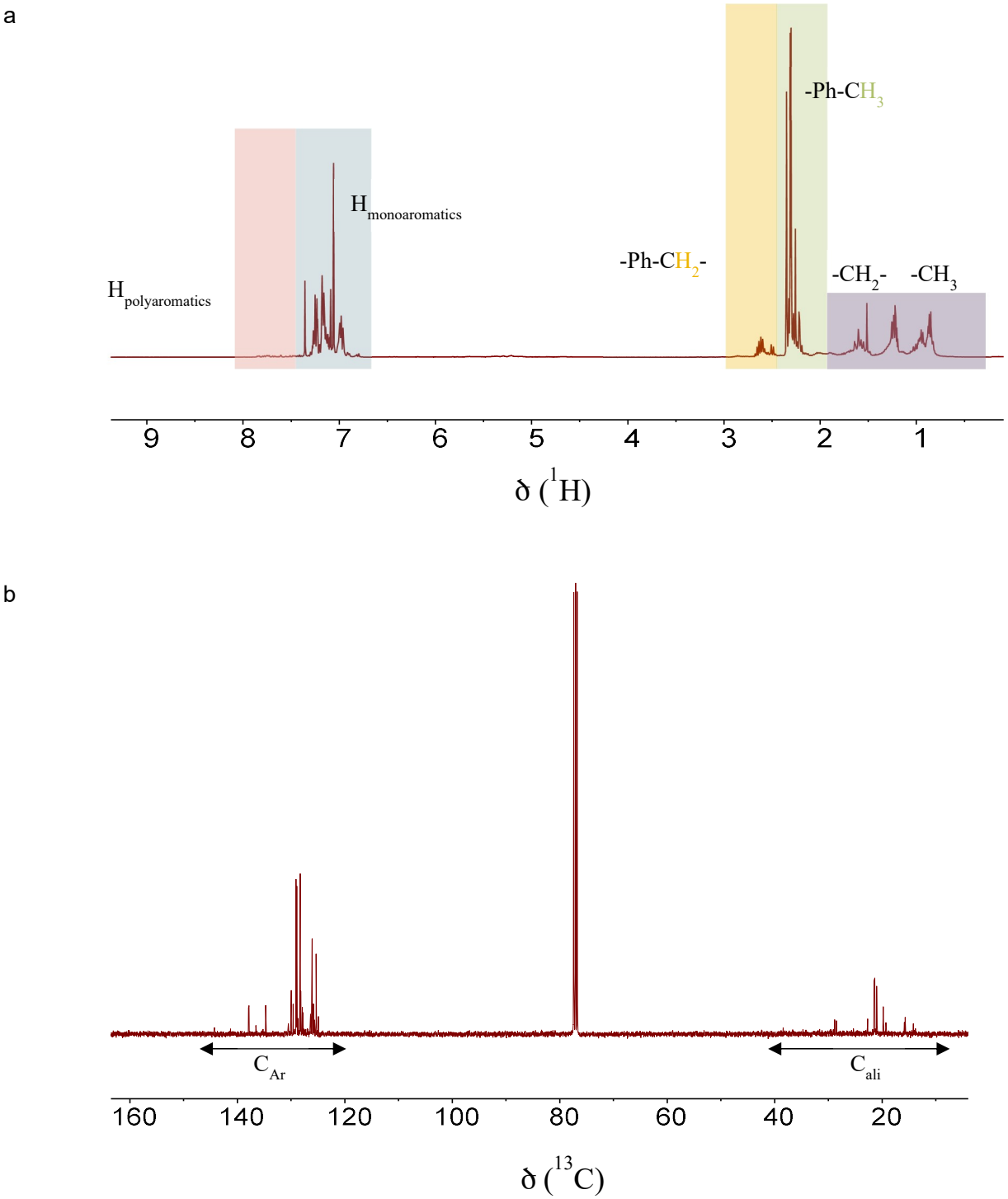

Figure S11. (a) ^{1}H and (b) ^{13}C NMR spectra of the liquid product.

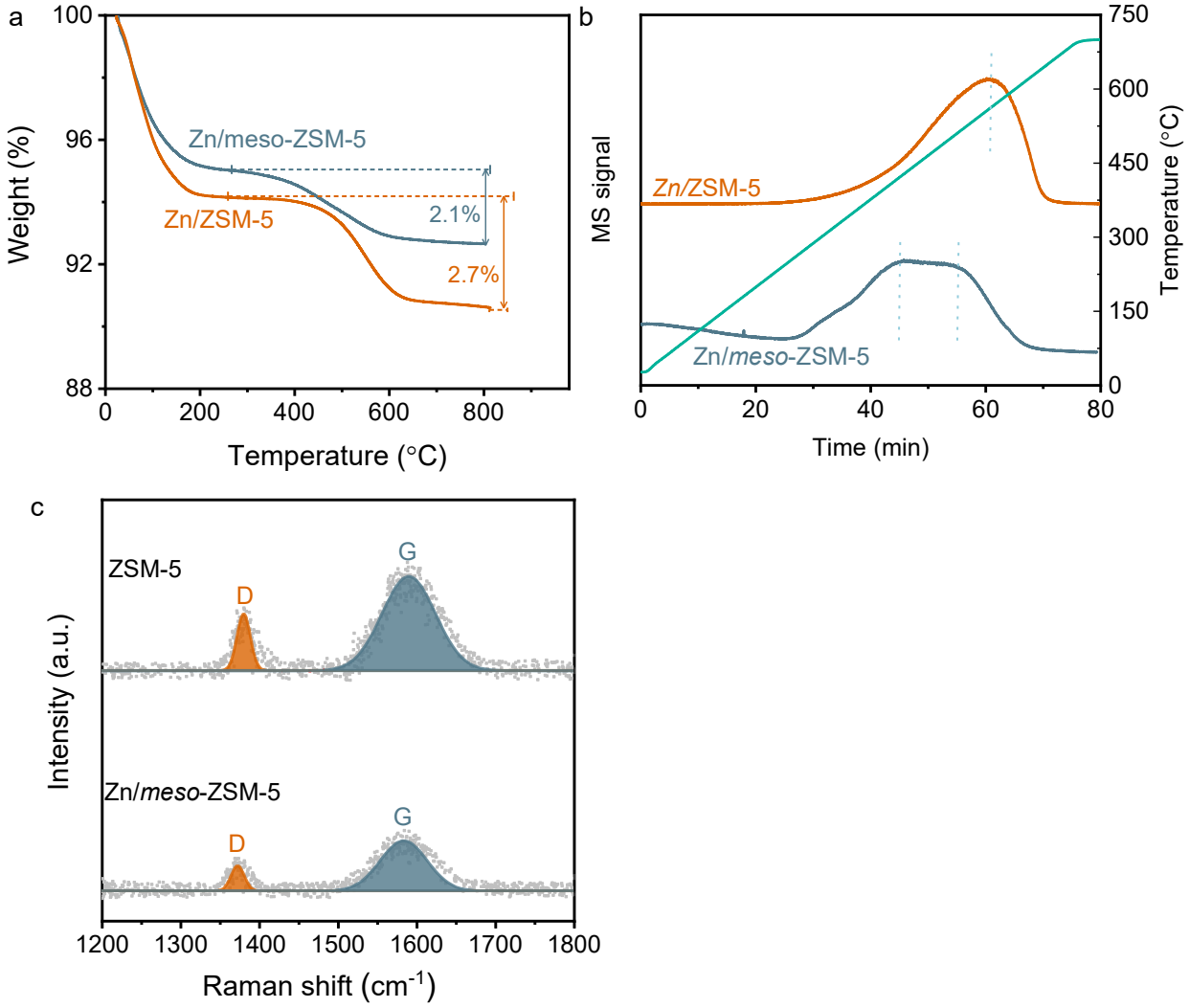

Figure S12. (a) TG and (b) TPO profiles of the used Zn/ZSM-5 and Zn/*meso*-ZSM-5. (c) Raman spectra of the spent Zn/*meso*-ZSM-5 catalyst with ZSM-5 catalyst as a reference. Reaction conditions: the mixture of 500 mg of PE and 100 mg of *s*-ZSM-5 in the first bed, 400 mg of catalyst for aromatization in the second bed, feed gas of 3.3% H_2/29.7% Ar/67% N_2, a flow rate of 3 mL/min, 400 °C, 4 h.

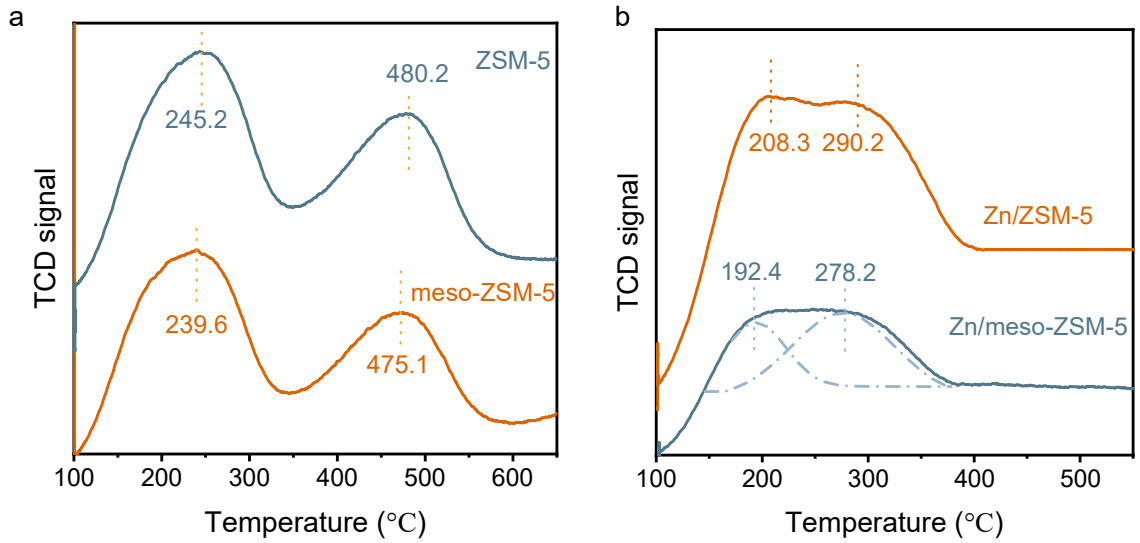

Figure S13. NH_3-TPD profiles of (a) *meso*-ZSM-5 and ZSM-5, (b) Zn/ZSM-5 and Zn/*meso*-ZSM-5.

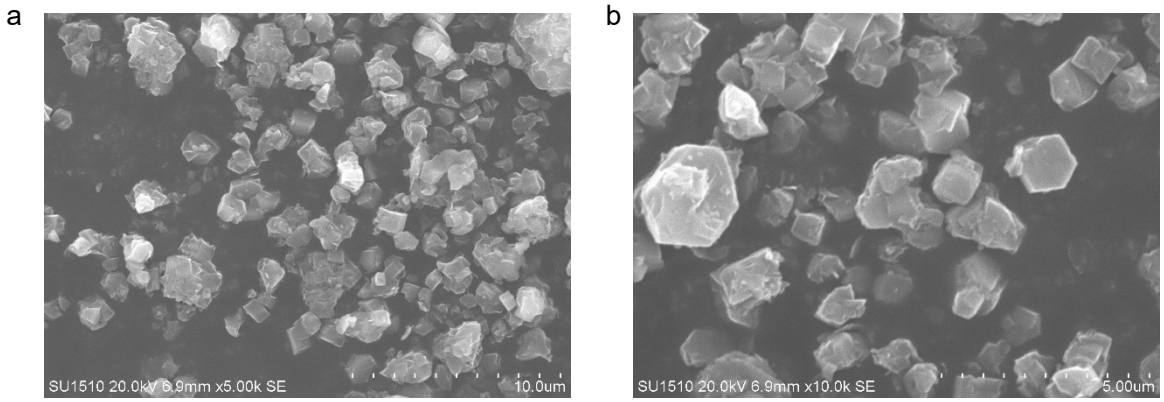

Figure S14. SEM images of Zn/*meso*-ZSM-5 zeolite.

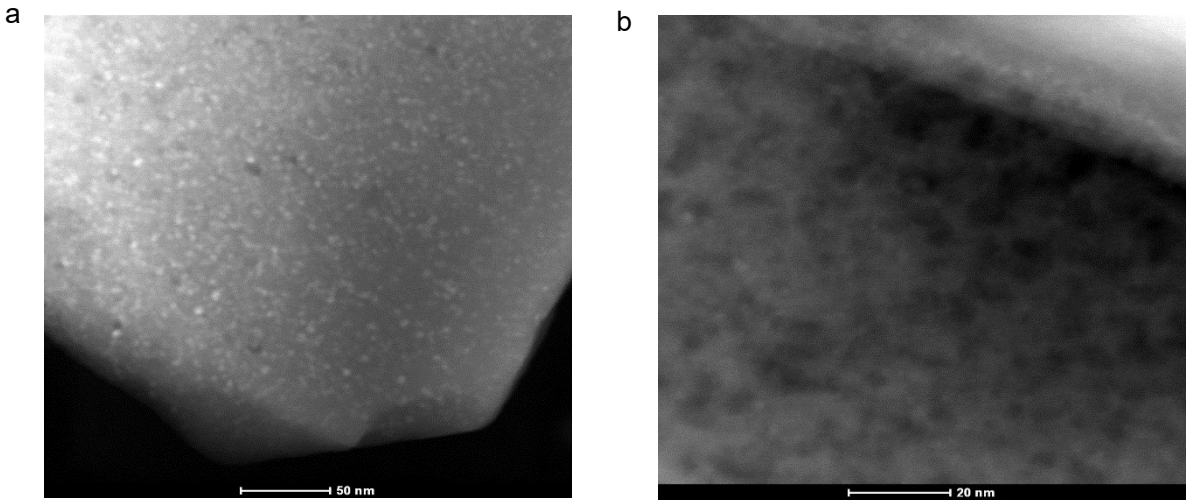

Figure S15. STEM images of (a,b) Zn/*meso*-ZSM-5 zeolite.

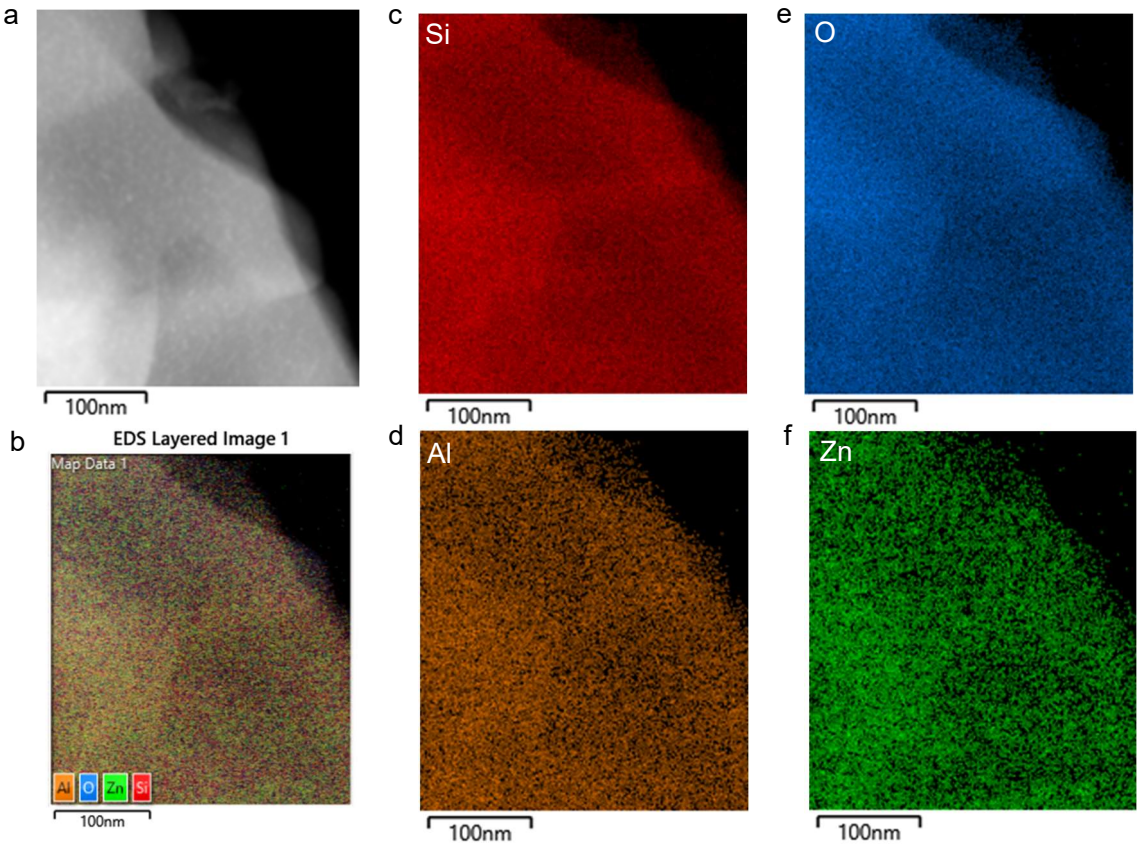

Figure S16. (a) STEM, (b) EDS, (c) Si, (d) Al, (e) O, and (f) Zn elemental maps of Zn/*meso*-ZSM-5.

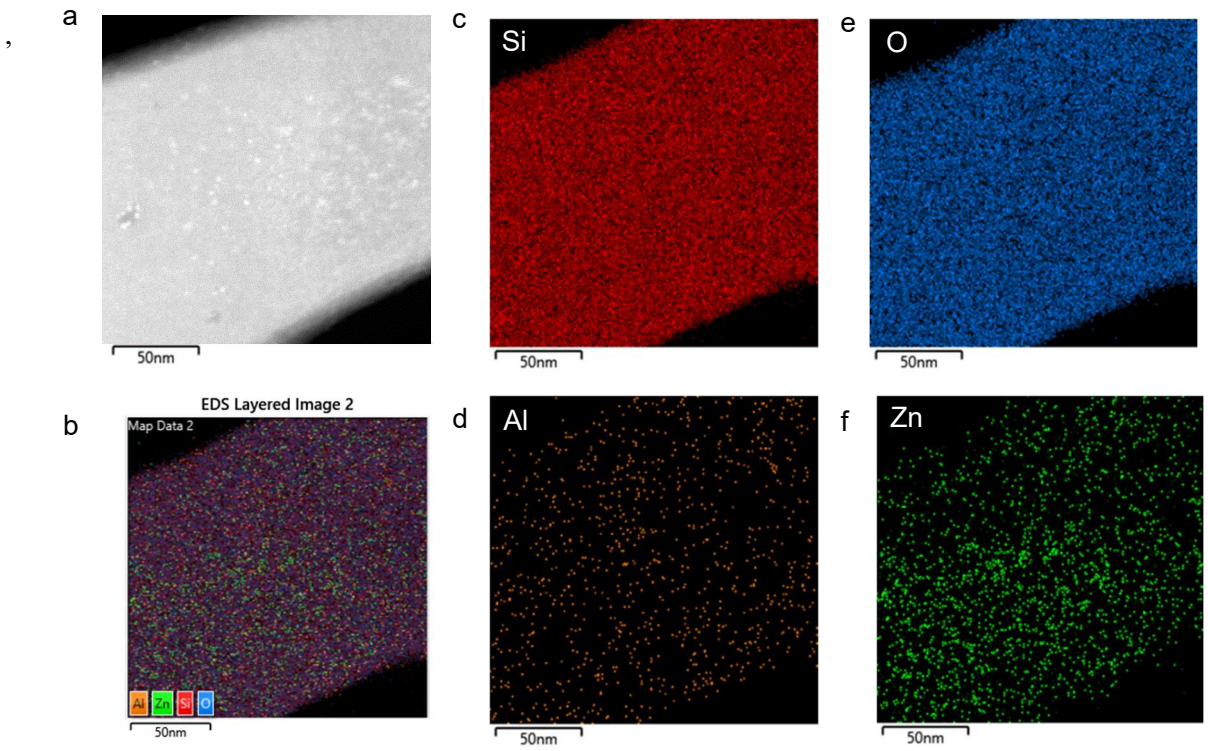

Figure S17. (a) STEM, (b) EDS, (c) Si, (d) Al, (e) O, and (f) Zn elemental maps of the Zn/*s*-ZSM-5.

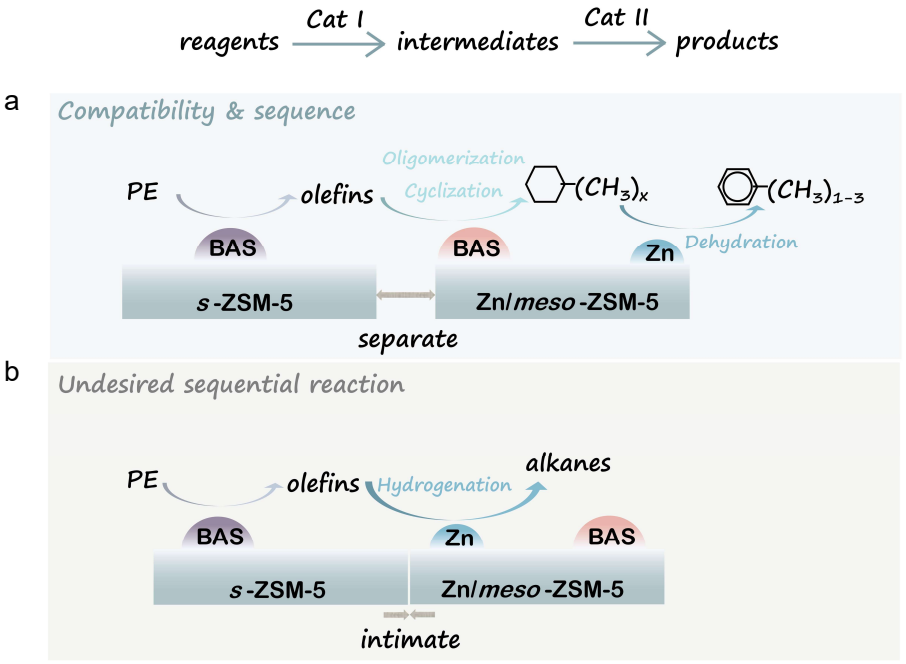

Figure S18. The distance required for efficient synergism between *s*-ZSM-5 and Zn/*meso*-ZSM-5.

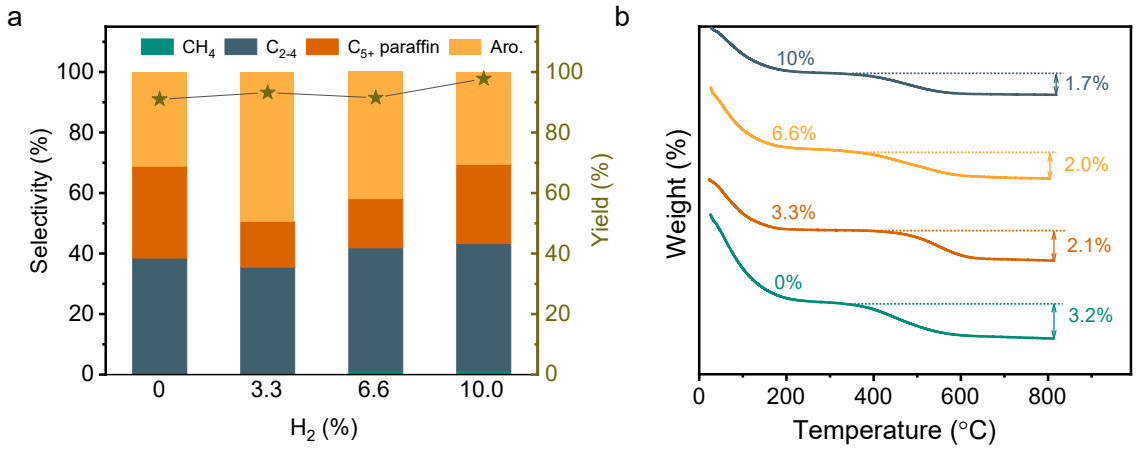

Figure S19. (a) Data characterization of the aromatization of PE over *s*-ZSM-5 and Zn/*meso*-ZSM-5 zeolite with different hydrogen content in the carrier gas. (b) TG profiles of the spent Zn/*meso*-ZSM-5 with different hydrogen content in the carrier gas. Reaction conditions: the mixture of 500 mg of PE and 100 mg of *s*-ZSM-5 in the first bed, 400 mg of Zn/*meso*-ZSM-5 for aromatization in the second bed, a flow rate of 3 mL/min, 400 °C, 4 h.

Note: Hydrogen is important for the reaction. In our previous study on *s*-ZSM-5 catalyzed PE conversion, the function of hydrogen has been experimentally and theoretically studied, which participate in the C-C cracking reaction and hindered the formation of the bulky molecule and polycyclic species in the micropores to ensure the free micropores for continuous reaction and diffusion, which is efficient to hinder the formation of coke/ oligomers that benefit the rapid mass transfer during catalysis. In addition, involving hydrogen in the feed has been used to hinder the coke formation in different reactions, such as MTO and STO.[14-19]

We performed the reaction using inert gas without hydrogen, and the hydrogen/nitrogen mixture with different hydrogen concentrations. As shown in figure S19, the reaction with inert nitrogen without hydrogen resulted in obviously reduced yields of aromatics. With 3.3 and 6.6% of hydrogen in the feed, the yield of aromatics was obviously higher than that in the hydrogen-free test. When 10% of hydrogen was used, the yields of aromatics were much lower with the formation of abundant light gases and C_{5+} alkanes, which might be due to the enhanced hydrogenation reaction that reduced the olefins into alkanes to hinder the aromatization. In addition, with the hydrogen participating in the reaction, the carbon deposition decreased significantly (Figure S19b).

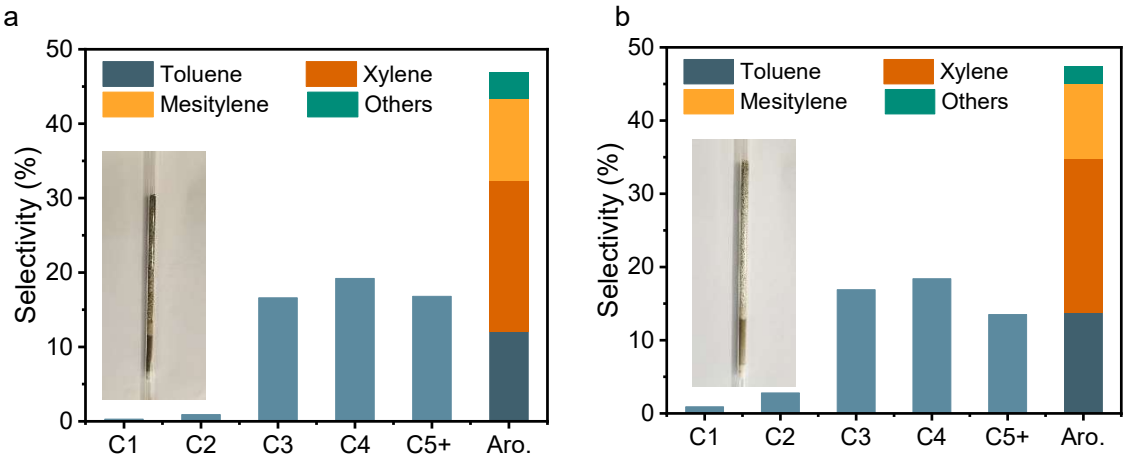

Figure S20. (a) Data characterization of the aromatization of the mixture of PE and PVC Reaction conditions: the mixture of 500 mg of PE, 50 mg of PVC, and 100 mg of *s*-ZSM-5 in the first bed, 400 mg of Zn/*meso*-ZSM-5 for aromatization in the second bed, feed gas of 3.3% H_2/29.7% Ar/67% N_2, a flow rate of 3 mL/min, 400 °C, and reaction for 4 h. (b) Data characterization of the aromatization of PE with inducing water over Zn/*meso*-ZSM-5. Reaction conditions: the mixture of 500 mg of PE and 100 mg of s-ZSM-5 in the first bed, 400 mg of Zn/meso-ZSM-5 for aromatization in the second bed, feed gas of 3.3% H_2/29.7% Ar/67% N_2, a flow rate of 3 mL/min, 400 °C, 4 h.

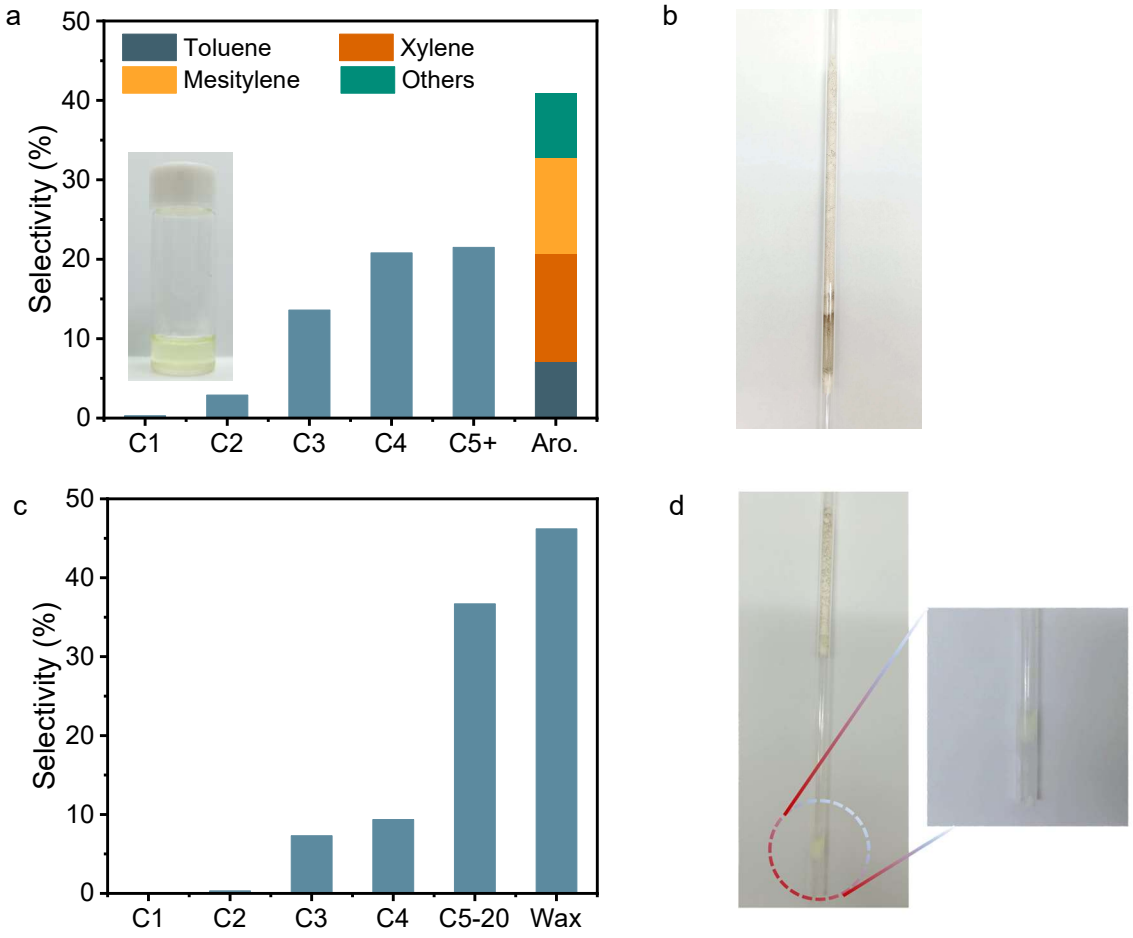

Figure S21. (a) Data characterization of the aromatization of PP over *s*-ZSM-5 and Zn/*meso*-ZSM-5. (b) Photograph showing the spent *s*-ZSM-5 and Zn/*meso*-ZSM-5. Reaction conditions: a mixture of 500 mg of PP and 100 mg of *s*-ZSM-5 in the first bed, 400 mg of Zn/*meso*-ZSM-5 for aromatization in the second bed, feed gas of 3.3% H_2/29.7% Ar/67% N_2, a flow rate of 3 mL/min, 400 °C, and reaction for 4 h. (c) Data characterizing the performance of *s*-ZSM-5 in PP depolymerization. (d) Photograph showing the spent *s*-ZSM-5 in the conversion of PP. Reaction conditions: a mixture of 500 mg of PP and 100 mg of *s*-ZSM-5, feed gas of 3.3% H_2/29.7% Ar/67% N_2, a flow rate of 3 mL/min, 400 °C, 4 h.

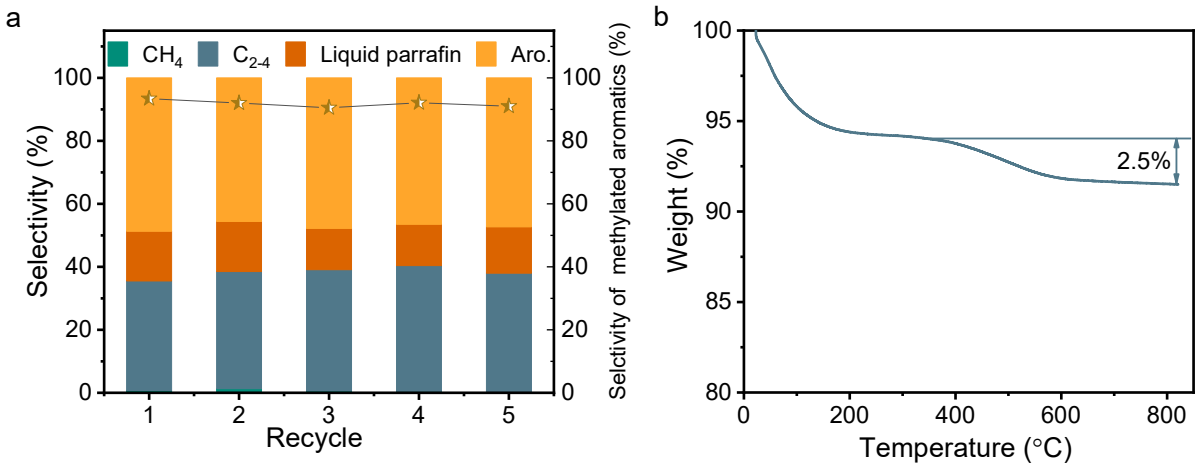

Figure S22. (a) Data characterization of the recyclability in polyethylene aromatization over *s*-ZSM-5 and Zn/*meso*-ZSM-5. Reaction conditions: the mixture of 500 mg of PE and 100 mg of *s*-ZSM-5 in the first bed, 400 mg of Zn/*meso*-ZSM-5 for aromatization in the second bed, feed gas of 3.3% H_2/29.7% Ar/67% N_2, a flow rate of 3 mL/min, 400 °C, and reaction for 4 h.

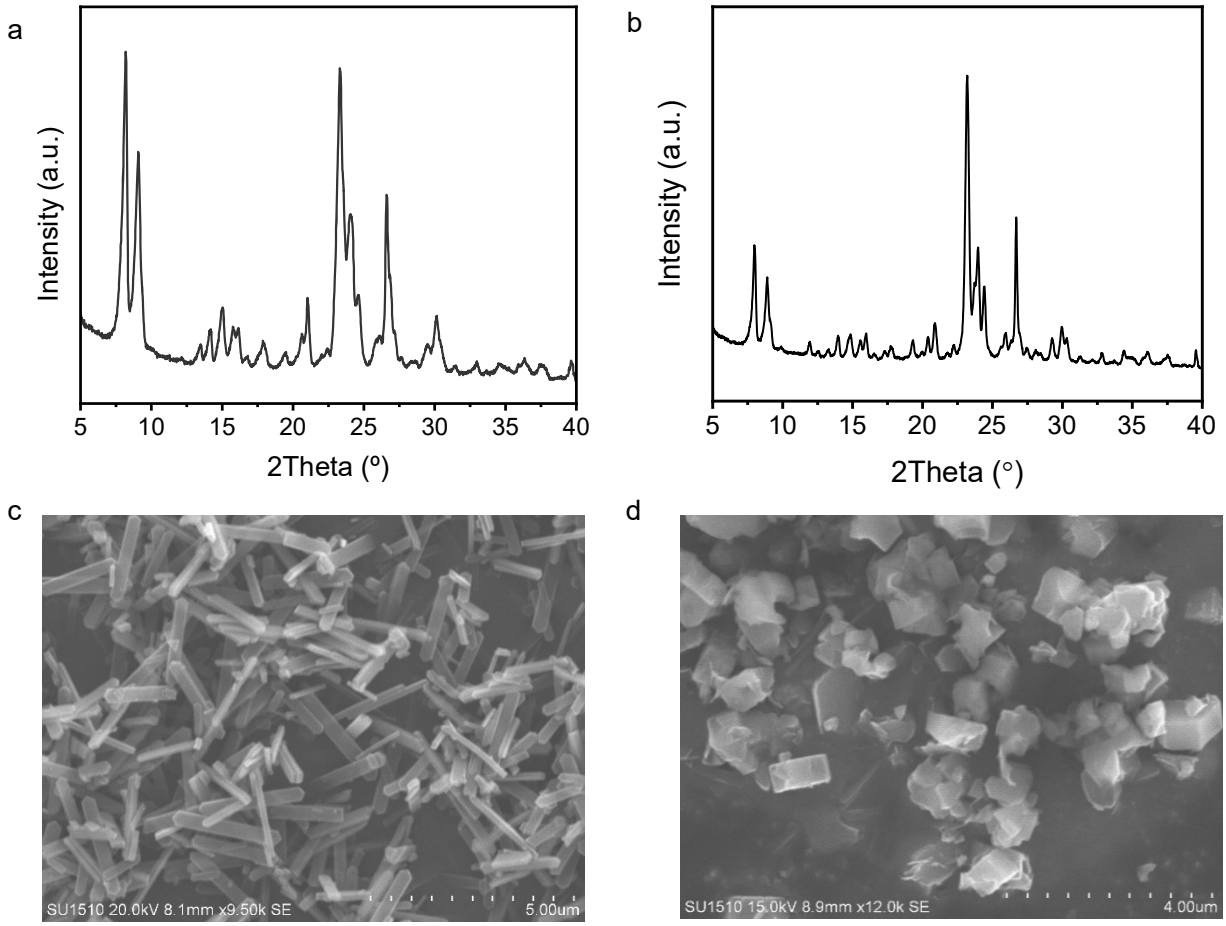

Figure S23. (a) XRD patterns and (c) SEM image of the spent *s*-ZSM-5 after 5 cycles. (b) XRD patterns and (d) SEM image of the spent *meso*-ZSM-5 after 5 cycles.

Table S1. Textural properties of ZSM-5 before and after treatment with different concentrations of aqueous NaOH solution.

Alkali concentration (mol/L)	S_{BET} (m^2/g)	S_{meso} (m^2/g)	V_{micro} (cm^3/g)	V_{meso} (cm^3/g)	D_{meso} (nm)
0	327.7	78.6	0.12	0.02	2.6
0.2	370.9	94.1	0.13	0.07	5.6
0.5	408.1	107.3	0.14	0.17	5.8
0.8	418.9	145.9	0.11	0.36	6.4

The mesoporous surface area was evaluated by the *t*-plot method. Pore volume for micropores and mesopores were evaluated by the *t*-plot method and BJH method, respectively. The mean pore diameter for mesopores was evaluated by the BJH method.

Table S2. Data characterization of polyethylene depolymerization over *s*-ZSM-5 and aromatization over *s*-ZSM-5 and Zn/*meso*-ZSM-5.

Catalyst	Yield of total product (%)	Selectivity (%)									
		CH_4	C_2	$C_2^=$	C_3	$C_3^=$	C_4	$C_4^=$	C_{5+}	$C_{5+}^=$	Aro.
s-ZSM-5	87.5	0.1	0.3	1.4	0.8	14.2	2.9	25.4	12.6	23.4	18.9
s-ZSM-5+ Zn/*meso*-ZSM-5	93.2	0.1	2.5	0.5	13.4	2.7	12.9	3.4	11.2	3.8	49.5

Reaction conditions: feed gas of 3.3% H_2/29.7% Ar/67% N_2, a flow rate of 3 mL/min, 400 °C, 4h.

Table S3. Benson group increments for various sub-groups.

Group label	Chemical identity	$\Delta_f H^o_{gas,est}$ (kJ mol^{-1})	$S^o_{gas,est}$ ($\times 10^{-3}$ kJ mol^{-1} K^{-1})
g_1	-CH_2-	-21.0	39.4
g_2	-CH_3	-42.7	127.2
g_3	=CH_2	26.2	33.4
g_4	=CH-C	35.9	42.7
g_5	CH_2-C=C	-20	41.0
g_6	C_{Ar}-CH_3	23.0	-32.1
g_7	C_{Ar}-H	14.0	48.2
g_8	Ring strain correction	3.0	-25.0
g_H	H_2	0	130.7

Table S4. Data characterization of polyethylene aromatization over various catalysts in Figure 1a.

Catalyst	Solid (%)	Yield of total product (%)	Selectivity (%)					Selectivity of C_{5+} (%)	
			CH_4	C_2	C_3	C_4	C_{5+}	Olefins and alkanes	Aro.
s-ZSM-5	12.5	87.5	0.1	1.7	15.0	28.3	54.9	65.5	34.5
n-ZSM-5	25.7	74.3	0.2	1.5	13.2	17.6	67.5	54.9	45.1
Zn/*n*-ZSM-5	22.7	78.3	0.3	1.5	13.8	21.2	63.2	47.5	52.5
s-ZSM-5 and Zn/ZSM-5*	7.9	92.1	0.2	2.1	17.9	23.5	56.3	54.1	45.9
s-ZSM-5 and Zn/ZSM-5	11.3	88.7	0.1	1.8	18.2	23.6	56.3	39.6	60.4
s-ZSM-5 and Zn/*meso*-ZSM-5	6.8	93.2	0.1	3.0	16.1	16.3	64.5	23.3	76.7
s-ZSM-5 and Zn/*s*-ZSM-5	19.7	70.3	0.1	2.0	14.4	25.0	58.5	51.1	48.9

Table S5. Data characterization of polyethylene aromatization over various catalysts in Figure 4c.

Entry[a]	Catalyst	Temp. (℃)	Yield of methylated aromatics (%)	Reference
1	ZSM-5	700	35.1	20
2	Fly ash	700	22.1	21
3	$ZnCl_2$	500	12.6	22
4	H_3PO_4-Activated Carbon	600	23.8	23
5	-	600	18.2	24
6	Spent FCC catalyst	400	8.7	25
7	ZSM-5 modification with boron	590	24.6	26
8	Sewage sludge derived char catalyst	600	14.0	27
9	Activated carbons	500	24.7	28
10	Zn-ZSM-11	500	29.2	29
11	Zn-activated carbons	526	32.0	30
12	H-Gallosilicate	425	15.4	31
13	Ni-ZSM-5	550	30.5	32
14	activated carbon	600	20.0	33
15	-	730	22.9	34
16	CaO and Ga/ZSM-5	500	29.2	35
17	HZSM5	450	9.1	36
18	HUSY	550	19.3	37
19	activated carbon	750	22.0	38
20	HZSM-5	500	10.0	39
21	ZSM-5	450	27.7	40
22	HZSM-5	500	22.0	41
23	CaO	719	18.0	42
24	ZSM-5	500	10.0	43
25	-	850	30.0	44
26	-	850	12.9	45
27	HUSY	600	6.9	46
28	-	700	22.0	47
29	-	700	7.0	48
30	Ga loaded HZSM-5	500	20.4	49
31	Co-pyrolysis	500	10.0	50
32	Conical spouted bed reactor	700	10.0	51

[a] The entries in Table S5 correspond to the numbers in Figure 4c in the main text.

Reference

1. S. W. Benson, F. R. Cruickshank, D. M. Golden, G. R. Haugen, H. E. O'Neal, A. S. Rodgers, R. Shaw and R. Walsh, *Chem. Rev.*, 1969, **69**, 279-324.
2. F. Zhang, M. Zeng, R. D. Yappert, J. Sun, Y. -H. Lee, A. M. LaPointe, B. Peters, M. M. Abu-Omar and S. L. Scott, *Science*, 2020, **370**, 437-441.
3. Y. Chung, F. H. Vermeire, H. Wu, P. J. Walker, M. H. Abraham and W. H. Green, *Journal of Chemical Information and Modeling*, 2022, **62**, 433-446.
4. J. Kang, K. Cheng, L. Zhang, Q. Zhang, J. Ding, W. Hua, Y. Lou, Q. Zhai and Y. Wang, *Angew. Chem. Int. Ed.* 2011, **50**, 5200-5203.
5. B. Zhao, P. Zhai, P.Wang, J. Li, T. Li, M. Peng, M. Zhao, G. Hu, Y. Yang, Y. -W. Li, Q. Zhang, W. Fan and D. Ma, *Chem*, 2017, **3**, 323-333.
6. Y. Li, S. Liu, Z. Zhang, S. Xie, X. Zhu and L. Xu, *Appl. Catal. A*, 2008, **338**, 100-113.
7. M. Bjørgen, F. Joensen, M. S. Holm, U. Olsbye, K. -P. Lillerud and S. Svelle, *Appl. Catal., A* 2008, **345**, 43-50.
8. Y. Song, X. Zhu, Y. Song, Q. Wang and L. Xu, *Appl. Catal. A*, 2006, **302**, 69-77.
9. J. Liang, L. Guo, W. Gao, C. Wang, X. Guo, Y. He, G. Yang and N.Tsubaki, *Ind. Eng. Chem. Res.*, 2022, **61**, 10336-10346.
10. X. Chen, Z. An, Y. Wang, Q. Ma, X. Feng, Y. Liu and C. Yang, *Fuel*, 2021, **290**, 119798.
11. Y. Fang, F. Yang, X. He and X. Zhu, *Front. Chem. Sci. Eng.*, 2019, **13**, 543-553.
12. N. Xu, D. Pan, Y. Wu, S. Xu, L. Gao, J. Zhang and G. Xiao, *React. Kinet. Mech. Catal.*, 2019, **127**, 449-467.
13. F. Zhou, Y. Gao, H. Ma, G. Wu and C. Liu, *Mol. Catal.*, 2017, **438**, 37-46.
14. S. S. Arora, D. L. S. Nieskens, A. Malek and A. Bhan, *Nature Catal.*, 2018, **1**, 666-672.
15. S. Lin, Y. Zhi, W. Zhang, X. Yuan, C. Zhang, M. Ye, S. Xu, Y. Wei and Z. Liu, *Chin. J. Catal.*, 2023, **46**, 11-27.
16. Y. Ni, Y. Liu, Z. Chen, M. Yang, H. Liu, Y. He, Y. Fu, W. Zhu and Z. Liu, *ACS Catal.*, 2019, **9**, 1026-1032.
17. S. S. Arora, Z. Shi and A. Bhan, *ACS Catal.*, 2019, **9**, 6407-6414.
18. X. Zhao, J. Li, P. Tian, L. Wang, X. Li, S. Lin, X. Guo and Z. Liu, *ACS Catal.*, 2019, **9**, 3017-3025.
19. M. DeLuca, C. Janes, and D. Hibbitts, *ACS Catal.*, 2020, **10**, 4593-4607.
20. P. Gaurh and H. Pramani, *Waste Manage.*, 2018, **71**, 86-96.
21. P. Gaurh and H. Pramani, *Waste Manage.*, 2018, **77**, 114-130.
22. K. Sun, Q. Huang, Y. Chi and J. Yan, *Waste Manage.*, 2018, **81**, 128-137.
23. K. Sun, Q. Huang, X. Meng, Y. Chi and J. Yan, *Energy Fuels*, 2018, **32**, 9772-9781.
24. S. -H. Jung, M. -H. Cho, B. -S. Kang and J. -S. Kim, *Fuel Process. Technol.*, 2010, **91**, 277-284.
25. K. -H. Lee, *Polymer Degradation and Stability*, 2008, **93**,1284-1289.
26. G. Zhou, J. Li, Y. Yu, X. Li, Y. Wang, W. Wang and S. Komarneni, *Applied Catalysis A: General*, 2014, **487**, 45-53.
27. K. Sun, N. J. Themelis, A. C. Bourtsalas and Q. Huang, *Journal of Cleaner Production*, 2020, **268**, 122038.
28. Y. Zhang, D. Duan, H. Lei, E. Villota and R. Ruan, *Applied Energy*, 2019, **251**, 113337.
29. M. S. Renzini, U. Sedran and L. B. Pierella, *Journal of Analytical and Applied Pyrolysis*, 2009, **86**, 215-220.
30. Y. Uemichi, Y. Makino and T. Kanazuka, *Journal of Analytical and Applied Pyrolysis*, 1989, **14**, 331-344.
31. U. Yoshio and S. Toshihiro, *Chemistry Letters.*, 1999, **28**, 1137-1138.
32. S. Zhou, P. Li, H. Pan and Y. Zhang, *Ind. Eng. Chem. Res.*, 2022, **61**, 11407-11416.
33. D. Zhang, X. Lin, Q. Zhang, X. Ren, W. Yu and H. Cai, *Energy*, 2020, **212**, 118983.
34. W. Kaminsky and J. -S. Kim, *Journal of Analytical and Applied Pyrolysis*, 1999, **51**,127-134.
35. L. Fu, Q. Xiong, Q. Wang, L. Cai, Z. Chen and Y. Zhou, *ACS Sustainable Chem. Eng.*, 2022, **10**, 9612-9623.

36. J. Aguado, D. P. Serrano, G. S. Miguel, M. C. Castro and S. Madrid, *Journal of Analytical and Applied Pyrolysis*, 2007, **79**, 415-423.
37. A. Marcilla, M. I. Beltrán and R. Navarro, *Applied Catalysis B: Environmental*, 2009, **86**,78-86.
38. D. Duan, Z. Feng, X. Dong, X. Chen, Y. Zhang, K. Wan, Y. Wang, Q. Wang, G. Xiao, H. Liu and R. Ruan. *Energy*, 2021, **232**, 121090
39. G. Elordi, M. Olazar, G. Lopez, M. Artetxe and J. Bilbao, *Ind. Eng. Chem. Res.*, 2011, **50**, 6061-6070.
40. X. Zhang, H. Lei, G. Yadavalli, L. Zhu, Y. Wei and Y. Liu, *Fuel.*, 2015, **144**, 33-42.
41. C. Muhammad, J. A. Onwudili and P. T. Williams, *Energy Fuels*, 2015, **29**, 2601-2609.
42. M. -H. Cho, S. -H. Jung and J. -S. Kim, *Energy Fuels*, 2010, **24**, 1389-1395.
43. M. Artetxe, G. Lopez, M. Amutio, G. Elordi, J. Bilbao and M. Olazar, *Ind. Eng. Chem. Res.*, 2013, **52**, 10637-10645.
44. F. J. Mastral, E. Esperanza, C. Berrueco, M. Juste and J. Ceamanos, *Journal of Analytical and Applied Pyrolysis*, 2003, **70**, 1-17.
45. C. Berrueco, F. J. Mastral, E. Esperanza and J. Ceamanos, *Energy Fuels*, 2002, **16**, 1148-1153.
46. M. d. R. Hernández, Á. N. García and A. Marcilla, *Journal of Analytical and Applied Pyrolysis*, 2007, **78**, 272-281.
47. G. Grause, S. Matsumoto, T. Kameda and T. Yoshioka, *Ind. Eng. Chem. Res.*, 2011, **50**, 5459-5466.
48. M. L. Mastellone, F. Perugini, M. Ponte and U. Arena, *Polymer Degradation and Stability*, 2002, **76**, 479-487.
49. J. Song, J. Wang, Y. Pan, X. Du, J. Sima, C. Zhu, F. Lou and Q. Huang, *Journal of Environmental Management*, 2022, **322**, 116096
50. S. Uçar, A. R. Özkan and S. Karagöz, *Journal of Analytical and Applied Pyrolysis*, 2016, **119**, 233-241.
51. G. Elordi, M. Olazar, G. Lopez, M. Artetxe and J. Bilbao, *Ind. Eng. Chem. Res.*, 2011, **50**, 6650-6659.